Interaction of Turing and Hopf bifurcations in chemical systems

Arkady Rovinsky* and Michael Menzinger

Department of Chemistry, University of Toronto, Toronto, Ontario, Canada M5S 1A1
(Received 27 January 1992)

When a Turing bifurcation occurs close to a Hopf bifurcation in the parameter space of a reaction-diffusion system, the Turing and Hopf modes may interact nonlinearly to form, *a priori*, a variety of complex spatiotemporal patterns. We have studied this type of interaction for three models of chemically active media: the Lengyel-Epstein model of the $ClO_2{}^- -I^-$ -malonic acid system, a model that describes the ferroin-catalyzed Belousov-Zhabotinsky reaction, and the Brusselator. One and two spatial dimensions are considered. The Poincaré-Birkhoff method was implemented for the reduction of the models to the Turing-Hopf normal forms. The normal-form analyses show that the stability regions of stationary periodic patterns and of homogeneous oscillations usually overlap over a wide region in parameter space, forming a domain of bistability. Mixed-mode (spatiotemporal) patterns do not occur in the models considered except for a very small region in the parameter space for two-dimensional hexagonal patterns.

PACS number(s): 05.70.−a, 47.20.Ky, 82.20.−w

I. INTRODUCTION

In his celebrated paper [1] Turing showed that the interplay of chemical reaction and diffusion may cause the homogeneous state of the system to become unstable and to lead to the spontaneous formation of spatially periodic stationary structures. He proposed this kind of instability as a possible mechanism for morphogenesis in biological systems and, more generally, for self-organization in nonlinear systems. The recent experimental discovery of Turing patterns in a real chemical system [2–4] has further stimulated the interest in self-organization phenomena and more detailed studies may be expected in the future.

Previous theoretical work [5,6] has shown that the closer the system is to the Hopf bifurcation point, the more the Turing instability is generally favored. The value of the diffusion coefficient ratio $\delta = D_x / D_y$ for which Turing instability becomes possible moves closer to one (the realistic value for homogeneous systems), as the Hopf boundary is approached. The proximity of these kinds of instability may lead to their interaction such that the resulting spatiotemporal pattern may significantly differ from the patterns that would appear in the case of either "pure" bifurcation. This fact should be important for the recognition, analysis, and classification of experimentally observed patterns.

The Turing bifurcation is associated with the passage of a real eigenvalue through zero (steady-state bifurcation), and the Hopf bifurcation with the crossing of the imaginary axis by a complex-conjugate pair of eigenvalues. Interactions of the Hopf and steady-state bifurcations may bring about a variety of complex kinds of behavior [7,8].

Here we study this type of interaction for models of three different chemical systems, the Lengyel-Epstein (LE) model [9] of the system for which Turing patterns have been found [2–4], the model that describes the ferroin-catalyzed Belousov-Zhabotinsky (BZ) reaction [13], and the Brusselator [15].

The work proceeds along the following lines. On the parametric plane, we find the degenerate point where both the Turing and Hopf bifurcations occur simultaneously. At this point, we reduce the model to the normal form implementing Birkhoff-Poincaré's method. Unfolding the normal form allows one to study the system in the vicinity of the degenerate bifurcation. The reduction to the normal form depends on the spatial geometry and dimensionality of the problem as well as on the boundary conditions. Here we consider only the cases of one and two spatial dimensions with no-flux (Neumann) boundary conditions. In two spatial dimensions, rather than generally analyzing the full range of possible patterns—a rather formidable task—we have restricted ourselves to considering several representative patterns. It is found that due to a bistability region, Turing patterns can exist over a much wider range of parameters than they would in the case of a pure Turing bifurcation. The conclusions reached for the LE model are found to hold equally for the BZ reaction and Brusselator models.

Section II presents the models, the normal forms, and the results of the calculations. Section III describes the derivation of the normal forms from the reaction-diffusion equations. A discussion of the results concludes the paper.

II. MODELS AND RESULTS

In this section we present the results of our calculations. General explanations of the approach and of the method used are given in the next section. We begin with the Lengyel-Epstein [9] model of the chlorite–iodide–malonic acid reaction since this model describes the medium in which Turing structures were observed experimentally [2–4].

The LE model is reduced to the following dimensionless form:

$$\frac{\partial x}{\partial \tau} = \alpha - x - 4\frac{xy}{1+x^2} + D_x \Delta x \ , \tag{1a}$$

$$\frac{\partial y}{\partial \tau} = \beta \left[x - \frac{xy}{1+x^2} \right] + D_y \Delta y \ , \tag{1b}$$

where

$$x = \frac{1}{\mu}[I^-], \quad y = \frac{1}{\nu}[ClO_2^-], \quad \tau = k_1 t \ ,$$

$$\mu = 10^{-7}, \quad \nu = \frac{\mu^2 k_2 [ClO_2^-]_0}{k_3 [I_2]_0} \ ,$$

$$\alpha = \frac{k_1 [A]_0}{k_2 [ClO_2^-]_0 \mu}, \quad \beta = \frac{k_3 [I_2]_0}{k_2 [ClO_2^-]_0 \mu} \ .$$

The quantities in brackets represent concentrations, and A denotes malonic acid. The rate constants are $k_1 = 7.5 \times 10^{-3} M^{-2} \ \mathrm{sec}^{-1}$, $k_2 = 6 \times 10^3 M^{-1} \ \mathrm{sec}^{-1}$, and $k_3 = 2.65 \times 10^{-3} \ \mathrm{sec}^{-1}$. The part of the model which describes the local kinetics has only two parameters α and β. Its parametric portrait is given in Fig. 1(a). The boundary separating the domains of homogeneous steady states and homogeneous oscillations is the locus of Hopf bifurcation labeled H.

In a full reaction-diffusion system (1), where the species are allowed to assume different values of the diffusivity, the homogeneous steady state may become unstable through the Turing bifurcation and give rise to a stationary spatially periodic pattern. The locus of Turing bifurcations is shown in Fig. 1(b), superimposed on the Hopf curve. The position of the Turing line is determined by the ratio $\delta = D_x / D_y$ of diffusion coefficients. Generally, the closer the value of δ is to 1, the narrower is the parameter domain where the homogeneous steady state can be destabilized only by inhomogeneous perturbations [the narrow region below the Turing and above the Hopf boundaries in Fig. 1(c)]. Since diffusion coefficients of small molecules are usually close to each other, the major part of parameter space where the Turing structures may occur overlaps the region of Hopf instability region. The Turing structures observed in the chlorite–iodide–malonic acid system [2–4] seem to be aided by immobilization of iodine species through starch that is present to act as an indicator. Even if the parameters lie in the nar-
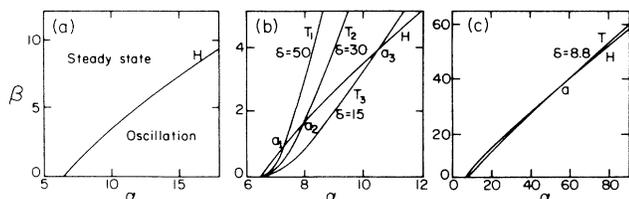
row region of the pure Turing instability, the proximity of the Hopf bifurcation may significantly affect the emerging spatial and/or temporal pattern. Therefore the understanding of these kinds of instability is important and relevant to the observed structures. As usual, the point of highest degeneracy constitutes the organizing center for interactions of this kind [10,11], whose unfolding leads to the complete description of the possible dynamics in its neighborhood. In our case, the point of double degeneracy lies at the intersection of the Turing and Hopf lines.

The dynamics of a system in the vicinity of a bifurcation point is governed by its normal form. Our task is therefore to derive and analyze the normal form for the degenerate Turing-Hopf bifurcation. This is done separately for spatial dimensions 1 and 2.

A. One-dimensional system

The calculations described in Sec. III show that the normal form for this case is

$$\dot{r} = \lambda r + ar^2 + bru^2, \quad \dot{u} = \mu u + cr^2 u + du^3 \ . \tag{2}$$

The r variable describes the Hopf mode and u the Turing model. The value of r characterizes the amplitude of the temporal oscillations (r is the radius of the limit cycle on the center manifold in the normal coordinates), while u represents the amplitude of the spatial pattern. Note that the r variable can only be positive while u may have either sign. However, Eq. (2) are invariant with respect to the sign of both variables. The bifurcation described by normal form (2) is called the pitchfork-Hopf bifurcation [7]. The coefficients a, b, c, and d of the normal form are calculated at the point of intersection of the lines of Turing and Hopf bifurcations (point a in Fig. 2). They depend on the system parameters α, β, δ, on the geometry of the problem, and on the boundary conditions as will be shown below. λ and μ are the unfolding parameters.

FIG. 1. The parameter plane of the Lengyel-Epstein model (1): H is the locus of Hopf bifurcation in the model without diffusion terms, T are the lines of Turing bifurcation for different values of δ [panels (b) and (c)].
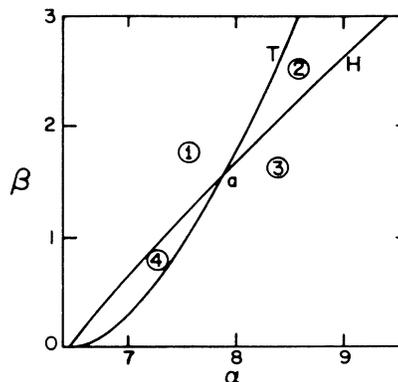

FIG. 2. The parameter plane for the reaction-diffusion system (1). Domain 1 is the region of the stable homogeneous steady state ($\lambda < 0$, $\mu < 0$). In domain 2 the homogeneous steady state is destabilized by the Turing mode ($\lambda < 0$, $\mu < 0$), and in domain 4, stability is lost through the Hopf mode ($\lambda > 0$, $\mu < 0$). Domain 3 ($\lambda > 0$, $\mu > 0$) is unstable both to Turing and Hopf modes.

For the LE model (1), the value of λ is negative above and positive below the Hopf boundary and the value of μ is negative above and positive below the Turing boundary (Fig. 2). The parameter plane is thus divided into four regions with different combinations of signs of λ and μ as illustrated in Fig. 2.

As illustrated in Figs. 1(b), and 1(c) the position of the point a is solely determined by the value of the diffusion ratio $\delta = D_x / D_y$: the smaller δ the further this point moves to large α. The coefficients a, b, c, and d are thus functions of $\alpha_a(\delta)$ and $\beta_a(\delta)$ while the unfolding parameters λ and μ are actually functions of the varying parameters α and β.

The dynamics of the normal form depends primarily on the sign of the parameter $\Delta = ad - bc$. Our calculations show that for the LE model (1), as well as for the BZ reaction and Brusselator models, as discussed in Sec. II C, Δ is always negative. This implies that from the set of dynamical modes that may arise a priori from the Turing-Hopf interaction only a subset actually occurs. It turns out that bistability between pure Turing and Hopf modes are the dominant result of this interaction. The more interesting cases of coupled Turing-Hopf (spatiotemporal) modes occur only for $\Delta > 0$.

The character of the bifurcation is controlled by the signs of the parameters a and d: negative a (or/and d) means that the Hopf (or/and Turing) bifurcation(s) is (are) supercritical; otherwise the corresponding bifurcation is subcritical. The influence of the diffusion ratio δ on the signs of ad and hence on the bifurcation character is illustrated by Fig. 3. When $\delta > \delta_2$ then the Turing line (not shown) intersects the solid portion of the Hopf line shown here, and $a,d > 0$, and both bifurcations are supercritical. Intersection in the dashed interval ab occurs for $\delta_1 < \delta < \delta_2$. For these δ values, $a < 0$ and $d > 0$, rendering the Hopf bifurcation supercritical and the Turing bifurcation subcritical. Both bifurcations become subcritical when the intersection occurs with the dash-dotted segment of the Hopf curve above the point b ($\delta < \delta_1, a, b < 0$).
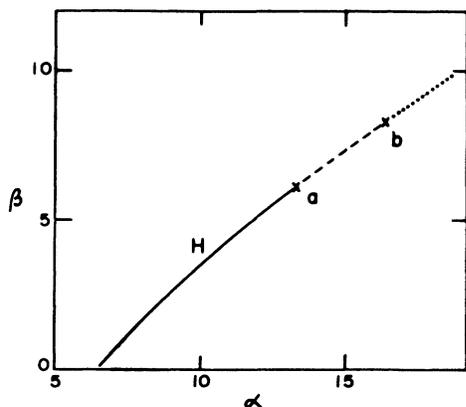

FIG. 3. When the Turing line intersects the solid portion of the Hopf line (below a; $\delta > 11.5$), both bifurcations are supercritical. When the crossing occurs in the dotted segment ab ($11.5 > \delta > 10.4$) then the Turing bifurcation is subcritical and the Hopf bifurcation is supercritical. Crossing above b ($\delta < 10.4$) makes both bifurcations subcritical.

It should be noted that in the subcritical Turing cases ($\delta < \delta_2$) spatial patterns may be accessed by threshold perturbations (hard excitation) in a limited domain in region 1 above the Turing line (Fig. 5). Similar circumstances apply to the subcritical Hopf case.

If $\Delta < 0$, as in all of the models analyzed in this paper, the normal form analysis can tell little about the asymptotic structures when both bifurcations are subcritical ($\delta < \delta_1$) or when Hopf is supercritical and Turing subcritical ($\delta_1 < \delta < \delta_2$), except that the locally stable steady state ($\lambda < 0$, $\mu < 0$) can always be destabilized by an appropriate finite perturbation. When $\delta_1 < \delta < \delta_2$ (supercritical Hopf and subcritical Turing) the same is true both for the region of the steady state ($\lambda < 0$, $\mu < 0$), and for the homogeneous limit cycle oscillations ($\lambda > 0$, $\mu < 0$). Only when both bifurcations are supercritical ($\delta > \delta_2$) can the analysis reveal more detail, as summarized in Fig. 4. In domain 1 where $\lambda, \mu < 0$, the homogeneous steady state is stable. Domain 2 corresponds to homogeneous oscillations. It consists of the region of pure Hopf instability ($\lambda > 0$, $\mu < 0$) bounded by H and T, and of the adjacent part of the region bounded by T and the line labeled B, where $\lambda, \mu > 0$. The latter boundary B is determined by

$$\lambda - \mu \frac{a}{c} = 0 , \tag{3}$$

where λ and μ are functions of the parameters α and β as explained above. The line of Turing bifurcation and the line A determined by

$$\lambda - \mu \frac{b}{d} = 0 \tag{4}$$

form the boundary of domain 3 where stationary, spatially periodic patterns exist. Region 4 between lines A and B is the domain of bistability. There the Turing pattern coexists with the homogeneous oscillation and initial conditions determine which of the two modes is realized.

If, in addition to the conditions $a, b, \Delta < 0$, the coefficients b and c were positive, then the stationary pattern in the domain $\lambda < 0$, $\mu > 0$ (domain 2 in Fig. 2) or the homogeneous oscillation in the domain $\lambda > 0$, $\mu < 0$ (domain 4 in Fig. 2) may not be globally stable and they could be destabilized by an appropriate hard-mode perturbation. However, this combination of parameters never occurs in any of the models considered here.

The main conclusion drawn from this section is that at least in the vicinity of the Turing-Hopf point a, the region where Turing patterns can be found is actually much larger than the narrow strip where only pure Turing structures exist. While the latter is bounded by the Turing line T from above and by the Hopf line H from below of Hopf bifurcation from the bottom, the former includes the domains 3 and 4 shown in Fig. 4.

B. Two-dimensional systems

While the spatial pattern in one spatial dimension is uniquely described by the wave vector k, in higher dimensions k_1, k_2 (and k_3 where applicable) may combine under different angles and with different amplitudes, giving rise to numerous spatial modes that have to be con-
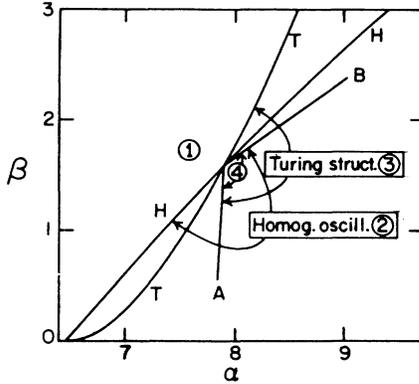
FIG. 4. The parameter plane for the one-dimensional system governed by Eq. (2).

sidered separately. Here we analyze only the simplest cases.

For two spatial dimensions the Turing-Hopf normal form is

$$\dot{r}=\lambda r+ar^3+br\sum_{|\mathbf{k}|=k_0}u_{\mathbf{k}}u_{-\mathbf{k}} \ , \tag{5a}$$

$$\dot{u}_{\mathbf{k}}=\mu u_{\mathbf{k}}+cr^2u_{\mathbf{k}}du_{\mathbf{k}}\sum_{|\mathbf{k}_1|=k_0}u_{\mathbf{k}_1}u_{-\mathbf{k}_1}$$

$$+e\sum_{\substack{\mathbf{k}_1+\mathbf{k}_2=\mathbf{k} \\ |\mathbf{k},k_1,k_2|=k_0}}u_{k_1}u_{k_2} \ , \tag{5b}$$

where u_k is the amplitude of the inhomogeneous mode with wave vector $\mathbf{k}$, and k_0 is the critical wave number (i.e., the wave number of the inhomogeneous perturbation which destabilizes the homogeneous steady state at $\mu\rightarrow+0$). The essential difference between this form and that (2) for 1D system is the presence of the last (quadratic) term in Eq. (5b). We are not aware of any published analysis of this normal form and begin by considering a few special cases.

One obvious solution to these equations is the one that describes Turing structures in the form of parallel rolls. In other words, the inhomogeneous mode depends only on a single spatial coordinate and it is characterized by a single wave vector $\mathbf{k}$. In this case system (5) is essentially one dimensional and it reduces to Eq. (2) analyzed in Sec. II A.

Another type of structure can be viewed as a superposition of two intersecting systems of rolls that form a rhombic pattern. This mode is determined by

$$U(\mathbf{r})=u_1\cos(\mathbf{k}_1\cdot\mathbf{r})+u_2\cos(\mathbf{k}_2\cdot\mathbf{r}) \ ,$$

$$(|\mathbf{k}_1|=|\mathbf{k}_2|=k_0) \ . \tag{6}$$

We assume that $u_1=u_2=u$. Since there are no modes with wave vectors $\mathbf{k}_1$, $\mathbf{k}_2$, and $\mathbf{k}_3$ such that $\mathbf{k}_1=\mathbf{k}_2+\mathbf{k}_3$, the quadratic term in Eq. (5b) becomes zero. Then the normal form (5) reduces again to Eq. (2), however, with different values of the parameters a, b, c, and d. Actual calculations show that in this case too the value of

$\Delta=ab-cd$ remains negative and the transitions from the sub to supercritical bifurcations occur almost at the same values of α as in the one-dimensional (1D) case (the difference lies within 10%; see Fig. 3). Therefore, the analysis and results of the previous section are applicable to the 2D case with only minor quantitative changes that are not of current interest.

A third type is a hexagonal pattern. Its complexities are more interesting. The hexagonal mode can be represented in the form

$$U(\mathbf{r})=u_1\cos(\mathbf{k}_1\cdot\mathbf{r})+u_2\cos(\mathbf{k}_2\cdot\mathbf{r})+u_3\cos(\mathbf{k}_3\cdot\mathbf{r}) \ , \tag{7}$$

where $|\mathbf{k}_1|=|\mathbf{k}_2|=|\mathbf{k}_3|=k_0$ and $\mathbf{k}_1+\mathbf{k}_2+\mathbf{k}_3=0$.

For regular hexagons $(u_1=u_2=u_3=u)$ the normal form (5) reduces to

$$\dot{r}=\lambda r+ar^3+bru^2, \quad \dot{u}=\mu u+cr^2u+du^3+eu^2 \ . \tag{8}$$

Calculations show that in this case too, the parameter $\Delta=ab-cd$ is always negative and the parameters a and d change their signs almost at the same value of α as in the previous cases.

It is known (Ref. [12] and references therein) that for $r=0$ (the pure stationary inhomogeneous mode) there can exist two different hexagonal structures differing only in their amplitudes. One is the small amplitude branch [soft mode, $u(\mu\rightarrow0)\rightarrow0$] and the other the large amplitude (hard-mode) branch, illustrated by Fig. 5. The interesting feature in the $d<0$ case is that the large amplitude branch remains stable at negative μ as long as $\mu>e^2/4d$.

Analysis of the normal form (8) leads to the following conclusions: the stability region of the homogeneous oscillations is defined by the inequalities

$$\lambda>0, \quad \mu=\lambda c/a<0 \ , \tag{9}$$

that of the large-amplitude stationary hexagonal structure by

$$\mu>\frac{e^2}{4d}, \quad \lambda+\frac{b}{2d^2}[e^2-2d\mu+e(e^2-4d\mu)^{1/2}]<0 \ , \tag{10}$$

and that of the small-amplitude pattern by

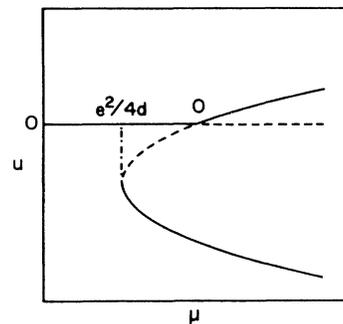$$\mu>0, \quad \lambda+b\frac{\mu^2}{e^2}<0 \ . \tag{11}$$

FIG. 5. The bifurcation diagram for the two-dimensional, hexagonal patterns (noninteracting with the Hopf mode).
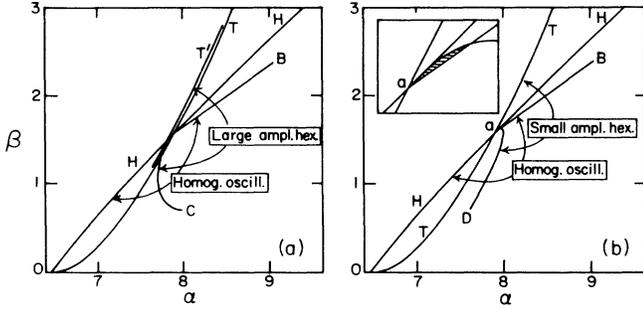
FIG. 6. The parameter plane for the system described by normal form (8): (a) the large-amplitude and (b) small-amplitude hexagonal structures interacting with the Hopf mode. The inset of 6(b) shows its central area magnified. The shaded region is the very small domain where the mixed-mode (oscillating hexagonal) pattern exists.

These cases are illustrated by Figs. 6(a) and 6(b).

Figure 6(b) demonstrates that there is a very small region near the degeneracy point a where neither the homogeneous steady state, nor the homogeneous oscillatory state or the small-amplitude stationary inhomogeneous structure are stable. Inside this tiny region, indicated by the shaded part of the inset of the figure, the normal form (8) has a stable steady state (r^*, u^*) with both r^* and u^* nonvanishing. This corresponds to a spatiotemporal mode where a hexagonal pattern with amplitude u^* undergoes temporal oscillations with amplitude r^*. This mixed-mode pattern, corresponding to a superposition of Turing and Hopf modes, has been simulated numerically and it is shown in Fig. 7.

A stable mixed-mode pattern may probably exist not only within that small region but in a wider area, presumably above the line B in Fig. 6, defined by $\mu = \lambda c / a < 0$. The comprehensive investigation of this possibility has not been completed.

C. The BZ reaction model and the Brusselator

The calculations were repeated for the BZ reaction model [13,14] and Brusselator [15] models, even though they do not appear as relevant to experiments as does the
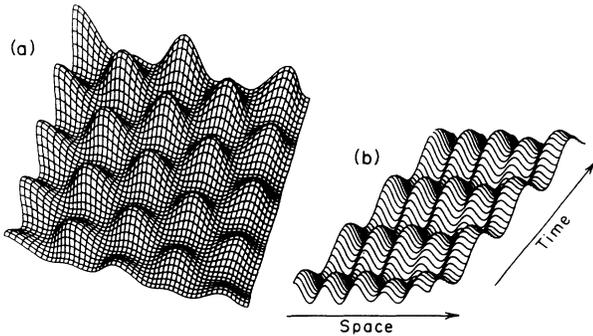

FIG. 7. The oscillating hexagonal (mixed-mode) pattern: (a) the spatial pattern at a fixed time [shaded area in Fig. 6(b)], (b) the time evolution of a one-dimensional cut through the structure shown in (a).

LE model. The BZ model describes quite accurately the ferroin-catalyzed BZ reaction. However, the appearance of the Turing structures seems unlikely in that system due to an inappropriate ratio of diffusion coefficients. The Brusselator is a purely formal model.

The important result of these calculations is that, just as in the Lengyel-Epstein model treated above, the normal form coefficients a and d, as well as $\Delta = ab - cd$, are always negative in the parameter regions considered. This means that the interaction of the Turing and Hopf bifurcations for these two models can only lead to the same behavior as that of the LE model described in the previous section.

III. REDUCTION TO THE NORMAL FORM

In this section we outline the ideas behind the Poincaré-Birkhoff reduction of the kinetic model (1) to the normal forms (2), (5), and (8).

Consider the reaction-diffusion system

$$\frac{d\mathbf{x}}{dt} = \mathbf{f}(\mathbf{x};p) + \hat{D}\Delta\mathbf{x} \tag{12}$$

near the homogeneous steady state $\mathbf{x}(r,t;p) = \mathbf{x}_0(p)$. Assume that at $p = p_0$ the system undergoes both the Hopf and Turing bifurcations. This means that the Jacobian $\hat{L} = \partial\mathbf{f}(\mathbf{x}_0(p_0);p_0)/\partial\mathbf{x}$ has a purely imaginary pair of eigenvalues and that the operator $\hat{L} - k^2 D$ has a zero eigenvalue at some k.

In some vicinities of p_0 one may expect that system (12) displays homogeneous oscillations,

$$\mathbf{x}(\mathbf{r},t;p) = \mathbf{x}_0(p_0) + \mathbf{x}^{(1)}(t;p) , \tag{13}$$

inhomogeneous stationary structures,

$$\mathbf{x}(\mathbf{r},t;p) = \mathbf{x}_0(p_0) + \mathbf{x}^{(2)}(\mathbf{r};p) , \tag{14}$$

and, generally, spatiotemporal structures,

$$\mathbf{x}(\mathbf{r},t;p) = \mathbf{x}_0 + \mathbf{x}^{(1)}(t) + \mathbf{x}^{(2)}(\mathbf{r},t) . \tag{15}$$

Expanding (12) as a Taylor series and retaining terms up to third order yields

$$\dot{\mathbf{x}}^{(1)} + \dot{\mathbf{x}}^{(2)} = \frac{\partial\mathbf{f}}{d\mathbf{x}}\sum_\alpha \mathbf{x}^{(\alpha)} + \hat{D}\Delta\mathbf{x}^{(2)}$$

$$+ \frac{1}{2}\frac{\partial^2\mathbf{f}}{\partial\mathbf{x}\partial\mathbf{x}}\sum_{\alpha,\beta}\mathbf{x}^{(\alpha)}\mathbf{x}^{(\beta)}$$

$$+ \frac{1}{6}\frac{\partial^3\mathbf{f}}{\partial\mathbf{x}\partial\mathbf{x}\partial\mathbf{x}}\sum_{\alpha,\beta,\gamma}\mathbf{x}^{(\alpha)}\mathbf{x}^{(\beta)}\mathbf{x}^{(\gamma)} + 0(4) , \tag{16}$$

where α, β, and $\gamma = 1,2$.

Now $\mathbf{x}^{(2)}(\mathbf{r},t)$ is expanded in a series of the eigenfunctions $I_i(r)$ of the operator $\hat{D}\Delta$,

$$\mathbf{x}^{(2)}(r,p) = \sum_i \mathbf{u}^{(i)}(t)I_i(r) . \tag{17}$$

We can choose the homogeneous eigenfunction $I_0(r) = \text{const} = 1$ and present

$$\mathbf{x}^{(1)}(t) = \mathbf{u}^{(1)}(t) . \tag{18}$$

Substituting (17) and (18) into (16), expanding the resulting products of I_i into series of $I_i(r)$ functions,

$$I_l(r)I_m(r) = \sum_{i=0} b_{lm}^{(i+1)} I_i(r) ,$$

$$I_l(r)I_m(r)I_n(r) = \sum_{i=0} C_{lmn}^{(i+1)} I_i(r) , \tag{19}$$

and disengaging the modes with different I_i gives

$$\dot{u}_i^{(\alpha)} = L_{ij}^{(\alpha)} u_j^{(\alpha)} + \frac{1}{2} \frac{\partial^2 f_i}{\partial x_j \partial x_k} b_{\beta\gamma}^{(\alpha)} u_j^{(\alpha)} u_k^{(\gamma)}$$

$$+ \frac{1}{6} \frac{\partial^3 f_i}{\partial x_j \partial x_k \delta x_l} c_{\beta\gamma\delta}^{(\alpha)} u_j^{(\beta)} u_k^{(\gamma)} u_l^{(\delta)} , \tag{20}$$

where $\alpha,\beta,\gamma,\delta = 1,2$,

$$L_{ij}^{(1)} = \frac{\partial f_i}{\partial x_j} , \quad L_{ij}^{(2)} = \frac{\partial f_i}{\partial x_j} - k_T^2 D_{ij} , \tag{21}$$

and k_T is the number at which $L_{ij}^{(2)}$ has a zero eigenvalue.

Since the $b_{\beta\gamma}^{(\alpha)}$ and $c_{\beta\gamma\delta}^{(\alpha)}$ matrices are determined by the eigenfunctions $I_i(r)$ they depend on the dimensionality, the geometry, and the boundary conditions of the problem. Here we consider only zero-flux (Neumann) boundary conditions and a rectangular geometry for the 2D case. Cosine eigenfunctions are appropriate in this case.

Thus, in the 1D case, the $b_{\beta\gamma}^{(\alpha)}$ and $c_{\beta\gamma\delta}^{(\alpha)}$ matrices are

$$b_{\beta\gamma}^{(\alpha)} = \begin{bmatrix} 1 & 0 \\ 0 & \frac{1}{2} \\ \\ 0 & 1 \\ 1 & 0 \end{bmatrix} , \tag{22}$$

$$c_{\beta\gamma\delta}^{(\alpha)} = \begin{bmatrix} 1 & 0 & 0 & \frac{1}{2} \\ 0 & \frac{1}{2} & \frac{1}{2} & 0 \\ \\ 0 & 1 & 1 & 0 \\ 1 & 0 & 0 & \frac{3}{4} \end{bmatrix} . \tag{23}$$

For the 2D rhombic structures the matrices are

$$b_{\beta\gamma}^{(\alpha)} = \begin{bmatrix} 1 & 0 \\ 0 & 1 \\ \\ 0 & 1 \\ 1 & 0 \end{bmatrix} , \tag{24}$$

$$c_{\beta\gamma\delta}^{(\alpha)} = \begin{bmatrix} 1 & 0 & 0 & 1 \\ 0 & 1 & 1 & 0 \\ \\ 0 & 1 & 1 & 0 \\ 1 & 0 & 0 & \frac{9}{4} \end{bmatrix} , \tag{25}$$

and for 2D hexagonal structures,

$$b_{\beta\gamma}^{(\alpha)} = \begin{bmatrix} 1 & 0 \\ 0 & \frac{3}{2} \\ \\ 0 & 1 \\ 1 & 1 \end{bmatrix} , \tag{26}$$

$$c_{\beta\gamma\delta}^{(\alpha)} = \begin{bmatrix} 1 & 0 & 0 & \frac{3}{2} \\ 0 & \frac{3}{2} & \frac{3}{2} & \frac{3}{2} \\ \\ 0 & 1 & 1 & 1 \\ 1 & 1 & 1 & \frac{15}{4} \end{bmatrix} . \tag{27}$$

Further calculations of the normal form are a cumbersome but straightforward implementation of the Poincaré-Birkhoff method as described, e.g., in Refs. [8,16]. The basic idea of the method is to find a nonlinear transformation of the variables $u_i^{(\alpha)}$ that reduces Eq. (20) to the simplest form by eliminating as many nonlinear terms as possible. The complex normal coordinates z and $\bar{z}$ that naturally appear in the Hopf mode are then replaced by real r and ϕ through substitution $z = r \exp(i\phi)$. Since the equation for ϕ is rather trivial it is not included in the normal forms (2), (5), and (8).

IV. THE NORMAL-FORM ANALYSIS

The detailed analysis of the normal form (2) has been reported in [8,17–21]. To illustrate the approach, we present the analysis for the following case: $\lambda, \mu > 0$; $a,b,c,d < 0$; $\Delta = ad - bc < 0$. We also discuss different kinds of spatiotemporal patterns that may plausibly be expected in systems governed by normal form (2), although it turns out that some of them ultimately do not occur in the three models studied.

For the case defined above, the normal form (2) always has three steady states: (I) $r_1 = u_1 = 0$ (the reference homogeneous steady state); (II) $r_2^2 = -\lambda/a, u_2 = 0$ (homogeneous oscillations); and (III) $r_3 = 0, u_3^2 = -\mu/d$ (stationary, spatially periodic pattern). The Jacobian matrix for these cases is

$$L = \begin{bmatrix} \lambda + bu_i^2 + 3ar_i^2 & 2bu_i r_i \\ 2cu_i r_i & \mu + cr_i^2 + 3du_i^2 \end{bmatrix} , \tag{28}$$

where u_i, r_i are the steady-state values $i = 1,2,3$. Thus the eigenvalues for these three cases are

(I) $\lambda, \mu > 0$ (the trivial steady state; always unstable) ,

(II) $-2\lambda \ (<0)$, $\mu - \lambda \dfrac{c}{a}$, $\tag{29}$

(III) $\lambda - \mu \dfrac{b}{d}$, $-2\mu \ (<0)$.

The steady state (II) (homogeneous oscillations) is stable when $\mu - \lambda c/a < 0$ and the stationary inhomogeneous structure [steady-state (III)] is stable when $\lambda - \mu b/d < 0$. Since $\Delta < 0$ it can be seen that the stability regions of the steady states (II) and (III) overlap so that the system is bistable when
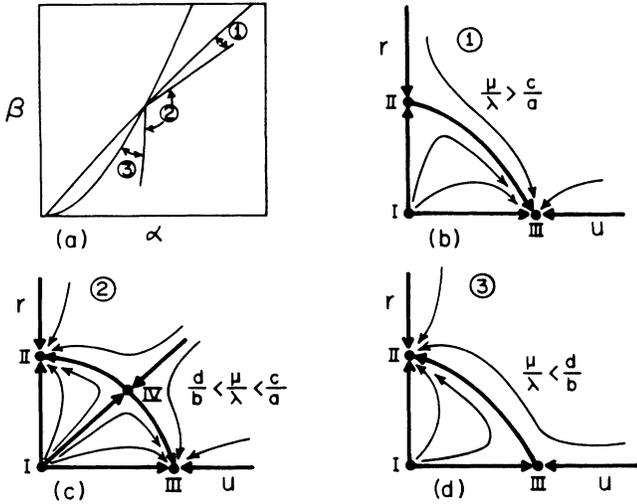
FIG. 8. The parameter plane (a) the phase portraits (b)–(d) of the normal form (2). The fixed points I, II, III are described by (29) and IV by (31).

$$\frac{d}{b} < \frac{\mu}{\lambda} < \frac{c}{a} \ . \tag{30}$$

Depending on the initial conditions it can be found either in the homogeneous oscillatory or inhomogeneous stationary state. When the inequalities (30) hold, a fourth steady state appears in the normal form:

$$(IV) \quad r_4^2 = \frac{-\lambda d + b\mu}{\Delta}, \quad u_4^2 = \frac{-\mu a + \lambda c}{\Delta} \ . \tag{31}$$

For the kinetic models considered in this paper this steady state is always unstable (a saddle point). As shown in Fig. 8(a) the parameter plane is divided into the three regions characterized by the phase portraits Figs. 8(b)–8(d).

All three kinetic models considered here are characterized by $\Delta < 0$. The emerging state of the system is therefore either homogeneously oscillating (Hopf bifurcation), or spatially periodic and stationary (Turing bifurcation). If Δ were positive, however, the steady state (IV) (r_4, u_4) of the normal form could become stable. This would correspond to the temporal oscillations of the Turing structure as a whole. If, in addition to $\Delta > 0$, the produce ad were negative this state would also become unstable and be surrounded by a stable limit cycle. Such limit cycle oscillations would correspond to doubly periodic oscillations of the inhomogeneous Turing structure such that both the mean value and the amplitude of the pattern oscillated with different frequencies. The analysis of normal form (8) is conducted in a similar fashion.

V. DISCUSSION

The most important result of this study is that the stability region of the inhomogeneous stationary patterns is generally much wider than the narrow strip where the pure Turing structures alone are stable, although in the major part of this stability region the patterns must coexist with the homogeneous oscillations. This fact has probably contributed to a great extent to the success of

the experiments in which the Turing patterns were discovered [2–4]. This also means that a domain of stable stationary patterns may be found within the oscillatory domain even when the pure Turing bifurcation never occurs (i.e., when the locus T of Turing bifurcations lies entirely within the oscillatory domain). The latter usually happens when the ratio δ of diffusion coefficients is close to 1—the common case for most chemical systems in solution. Moreover, although the necessary condition for the pure Turing instability is that the diffusion coefficient of the "inhibitor" should exceed that of the "activator" [24], the present results imply that even when this condition is not met, there may be substantial regions within the oscillating domain where inhomogeneous patterns coexist with homogeneous (limit cycle) oscillations.

It remains puzzling why the analyses of the three quite different kinetic models have consistently shown that the Turing structures in 1D and the 2D roll and rhombic structures never couple with the Hopf mode to yield temporally oscillating inhomogeneous (mixed-mode) patterns. The appearance of the oscillations or double-periodic oscillations of the inhomogeneous mode is determined by the coefficients of the normal forms (2) or (5). These coefficients are not fully independent since they all derive from the same original equations. It is not yet clear under which physical conditions the system would be characterized by the normal form with $\Delta = ad - bc > 0$ (which may exhibit periodic oscillations of the spatial structure) and with $ad < 0$ (leading to doubly periodic oscillations).

In the course of this work we made a series of simplifications and have left several interesting problems unsolved. In the 2D case in particular, we did not consider the large class of patterns with an arbitrary angular distribution of wave vectors and with different amplitudes in the different directions of the wave vectors. The analyses for these cases will be more intricate, but their dynamics promise to be of interest. It is likely, furthermore, that the full three-dimensional system possesses a bifurcation structure that is not completely captured by the present 1D and 2D cases.

The stability analysis was limited only to homogeneous perturbations and perturbations with the wave vector of the Turing mode. It was shown earlier [22,23] that small arbitrary inhomogeneous perturbations can destabilize the homogeneous oscillations and lead to the onset of high-dimensional chaos. They are also important for the stability of the inhomogeneous stationary structure (Ref. [12] and references therein), although the comprehensive analysis even in this case has not been completed. In our case the implications can be even more significant.

The present approach does not allow one to find all the final destinations of the system in the case of subcritical bifurcations. One can expect, however, that in the vicinity of the point where the bifurcation changes from supercritical to subcritical (where a or d changes its sign), the emerging structure and its stability will be qualitatively similar to the supercritical cases. A thorough analysis may reveal further interesting and relevant aspects of the problem.

*On leave from the Institute of Theoretical and Experimental Biophysics of the Academy of Sciences, Puschino, Moscow Region, 142292, Commonwealth of Independent States.

[1] A. M. Turing, Philos. Trans. Soc. London Ser. B **327**, 37 (1952).

[2] V. Castets, E. Dulos, J. Boissonade, and P. De Kepper, Phys. Rev. Lett. **64**, 2953 (1990).

[3] P. De Kepper, V. Castets, E. Dulos, and J. Boissonade, Physica D **49**, 161 (1991).

[4] Q. Ouyang and H. Swinney, Nature **352**, 610 (1991).

[5] A. B. Rovinsky, J. Phys. Chem. **91**, 4606 (1987).

[6] J. E. Pearson and W. Horsthemke, J. Chem. Phys. **90**, 1588 (1989).

[7] W. F. Langford, in *Nonlinear Dynamics and Turbulence,* edited by G. Barenblatt, G. Iooss, and D. D. Joseph (Pitman, London, 1985), pp. 215–237.

[8] S. Wiggins, *Introduction to Applied Nonlinear Dynamical Systems and Chaos* (Springer-Verlag, New York, 1990).

[9] I. Lengyel and I. R. Epstein, Science **251**, 650 (1991).

[10] R. Thom, *Structural Stability and Morphogenesis* (Benjamin, Reading, MA, 1975).

[11] J. Guckenheimer, Physica D **20**, 1 (1986).

[12] B. A. Malomed and M. A. Tribelski, Zh. Eksp. Teor. Fiz. **92**, 539 (1987) [Sov. Phys.—JETP **65**, 305 (1987)].

[13] A. B. Rovinsky and A. M. Zhabotinsky, J. Phys. Chem. **88**, 6081 (1984).

[14] R. R. Aliev and A. B. Rovinsky, J. Phys. Chem. **96**, 732 1992.

[15] G. Nicolis, and I. Prigogine, *Self-Organization in Nonequilibrium Systems* (Wiley-Interscience, New York, 1977).

[16] V. I. Arnold, *Geometrical Methods in the Theory of Ordinary Differential Equations* (Springer-Verlag, New York, 1983).

[17] G. P. Keener, Stud. Appl. Math. **55**, 187 (1976).

[18] P. Holmes, Ann. N.Y. Acad. Sci. **357**, 473 (1980).

[19] G. Iooss and W. F. Langford, Ann. N.Y. Acad. Sci. **357**, 489 (1980).

[20] W. F. Langford, in *Dynamical Systems,* edited by A. R. Bednarek, and L. Cesari (Academic, New York, 1982).

[21] W. F. Langford and G. Iooss, in *Bifurcation Problems and their Numerical Solutions,* edited by H. D. Mittelmann and H. Weber (Birkhauser Verlag, Basel, 1980), pp. 103–134.

[22] Y. Kuramoto, *Chemical Oscillations, Turbulence and Waves* (Springer-Verlag, Berlin, 1984).

[23] A. B. Rovinsky, J. Phys. Chem. **94**, 7261 (1990).

[24] L. Segel and J. L. Jackson, J. Theor. Biol. **37**, 545 (1972).